Materials Today Sustainability 34 (2026) 101367

Contents lists available at ScienceDirect

Materials Today Sustainability

journal homepage: www.journals.elsevier.com/materials-today-sustainability

Photocatalysts and EOs could they ever be friends? A coating for stone materials

Andrea Campostrini [a,e], Teresa Botrè [a], Elena Ghedini [b,a], Sabrina Manente [a], Alex W. Robertson [c], Pilar Bosh-Roig [d], Federica Menegazzo [a,*], Michela Signoretto [a]

[a] Department of Molecular Sciences and Nanosystems, Ca' Foscari University of Venice and INSTM RUVe, Via Torino 155, Venice, 30172, Italy
[b] Department of Chemistry, University of Bari Aldo Moro, Via Edoardo Orabona 4, Bari, 70121, Italy
[c] Department of Physics, University of Warwick, Coventry, CV4 7AL, United Kingdom
[d] Instituto Universitario de Restauración del Patrimonio, Universitat Politècnica de València, Camí de Vera s/n, Valencia, 46022, Spain
[e] Center for Cultural Heritage Technology, Istituto Italiano di Tecnologia, Via Adriano Olivetti 1, Roncade, 31056, Italy

ARTICLE INFO

Keywords:
Titanium dioxide (TiO_2)
Silica nanocontainers
Photocatalytic coating
Antimicrobial
Hybrid hydrogel

ABSTRACT

This study presents the formulation of a hybrid protective coating for stone materials, designed to provide both photocatalytic and antimicrobial properties by leveraging the synergistic combination of titanium dioxide (TiO_2) photocatalytic nanoparticles with mesoporous silica (SiO_2) MCM-41 nanocontainers loaded with *Origanum compactum* essential oil (EO). The ordered mesoporous SiO_2, enriched with TiO_2 nanoparticles, serves as carried for the EO, while a hybrid hydrogel composed of chitosan and a mixture of silicon alkoxides (MTES and TEOS) is used to formulate the protective coating. The coating was applied to stone mock-ups, and its performance was evaluated in terms of hydrophobicity, water permeability, colorimetric changes, and antimicrobial efficacy. The results demonstrated that the coating effectively combined photocatalytic, antimicrobial, and self-cleaning functionalities, offering a sustainable and high-performance solution for the preservation of heritage materials while minimizing environmental impact and risks to operators.

1. Introduction

Stone materials, such as granite, limestone, sandstone, and marble, are widely used in the construction and architectural sector due to their durability and aesthetic properties. However, these materials are prone to degradation through several weathering mechanisms, with mechanical, chemical, and biological agents leading to structural and aesthetic deterioration [1–3]. The protection of stone surfaces is therefore critical, especially for those exposed outdoors [4]. In addition to preserving structural integrity and aesthetic value, effective protection of stone surfaces can significantly reduce maintenance and cleaning costs over time, while helping to preserve cultural heritage, including historic monuments and artworks. Furthermore, environmentally friendly protective strategies are increasingly required to minimize chemical exposure and operator risks, motivating the development of sustainable coatings [5].

In this context, protective coatings play a crucial role in avoiding direct contact with the substrate and enriching the surface with innovative useful features [6]. Ideally, protective coatings should be durable, transparent, non-toxic for the operator, sustainable, and hydrophobic while permeable to water vapor [7–10]. Water is one of the principal factors that leads to several deterioration phenomena; among these, biodeterioration plays a crucial role [11,12]. For this reason, another aspect that a protective coating should have is the ability to inhibit microbiological growth [13,14].

Recent advancements in nanotechnology have led to the development of innovative coatings, based on nanostructured materials, that enhance the self-cleaning and protective properties of treated surfaces [15–18]. Photocatalytic materials, when exposed to light radiation, generate Reactive Oxygen Species (ROS) such as O^{2-}, HO_2, and $OH^{\cdot}$. The most studied photocatalyst is titanium dioxide (TiO_2), which is a well-known material with excellent photocatalytic and self-cleaning properties, making it suitable also for stone protection [19–23]. The photocatalytic activity can deteriorate the damaging organic materials

* Corresponding author.
E-mail addresses: andrea.campostrini@unive.it (A. Campostrini), teresa.botre@unive.it (T. Botrè), elena.ghedini@uniba.it (E. Ghedini), mantente@unive.it (S. Manente), alex.w.robertson@warwick.ac.uk (A.W. Robertson), mabosroi@upvnet.upv.es (P. Bosh-Roig), federica.menegazzo@unive.it (F. Menegazzo), miky@unive.it (M. Signoretto).

https://doi.org/10.1016/j.mtsust.2026.101367
Received 5 July 2025; Received in revised form 26 January 2026; Accepted 23 April 2026
Available online 14 May 2026

deposited on the surface, keeping it cleaner for a longer time. Strictly linked to its photocatalytic activity, it has also been investigated for its antimicrobial properties in several fields of application, with ROS able to attack and degrade microorganisms' cellular components, including membranes and DNA [24–27]. Nevertheless, due to its white coloration, its application in the cultural heritage field is still challenging.

Another interesting sustainable way to combat biodeterioration is the use of natural substances, such as essential oils (EOs) [28–31]. Their wide and high concentration of active molecules makes them good candidates to act as antimicrobial agents against the microorganisms that easily proliferate on stone surfaces [32,33]. Nevertheless, the high volatility of their active molecules and the risk of surface staining have limited their use primarily to cleaning interventions, where contact with the substrate is brief, potentially preventing the full exploitation of their properties. In this sense, different ways for their embedding into nanostructured matrices or polymers have been studied for applications in the industrial pharmaceutical field, whereas their use in restoration is still a developing novelty [34–36]. Several studies have explored SiO_2-TiO_2 nanocomposite coatings for stone protection, focusing on photocatalytic, self-cleaning, and antimicrobial properties [37–41]. While these works demonstrate effective degradation of organic deposits and partial microbial inhibition, most coatings lack long-term biocidal activity or require repeated application. Very few studies have addressed the integration of natural antimicrobial agents, such as essential oils, into these matrices. The incorporation of essential oils (EOs) into nanocapsules represents a novel strategy to enhance antimicrobial performance while maintaining self-cleaning and photocatalytic functionalities. In this regard, nanocapsules of ordered mesoporous silica (SiO_2) are a perfect candidate. Mesoporous materials are known for their ability to interact with ions and molecules on both their external and internal surfaces, making them able to encapsulate and later release an active agent [42–44]. For this feature, they are highly investigated in several fields of application, especially as drug delivery systems (DDS). These materials are produced through the self-assembly of surfactants, which mold the inorganic component and are characterized by an ordered mesostructure, high surface area, and well-defined properties, making them ideal for encapsulating molecules of all kinds, from proteins to drugs to biocides [45]. Mesoporous silicas, such as MCM-41, are highly efficient matrices in the design of controlled release systems due to characteristics like pore size, ordered structure, and easily functionalizable or tunable surfaces [42,46].

This study focuses on the development of a novel hybrid protective coating based on mesoporous silica MCM-41 nanocontainers, enriched with TiO_2 and loaded with *Origanum compactum* essential oil. These materials would be then embedded in an organic-inorganic hybrid matrix composed of chitosan and a mixture of silicon alkoxides (methyltriethoxysilane and tetraethylorthosilicate). The presence of a photocatalyst in the mixture would not only prolong the biocide effect but also ensure air pollutants abatement and a self-cleaning effect on the stone surface. However, a question is raised; would photocatalytic TiO_2 and oregano EO act in conflict or cooperate in a synergistic action?

2. Materials and methods

The protective coating was developed through a multi-step process, beginning with the synthesis of mesoporous silica (MCM-41), the subsequent impregnation with titanium dioxide (TiO_2) nanoparticles and essential oil of oregano, and finally the formulation of the hybrid hydrogel matrix.

2.1. Reagents

Here we report the reagents employed for the synthesis of silica mesoporous MCM-41, its impregnation, and the formulation of the coating. Tetraethyl orthosilicate (TEOS; CAS 78-10-4), reagent grade, 98%, from Sigma-Aldrich® (Merck Life Science S.r.l., Milan, Italy); hexadecyltrimethylammonium bromide (CTAB; CAS 57-09-0), ≥99.0% (AT), from Thermo Scientific Chemicals (Thermo Fisher Scientific Inc., Waltham, Massachusetts, USA); NaOH (CAS 1310-73-2) flakes, reagent grade, 97%, from Sigma-Aldrich® (Merck Life Science S.r.l., Milan, Italy); TiO_2 P25 (CAS 13463-67-7), nanopowder, ≥99.5%, from Evonik Industries AG (Essen, Germany); TiO_2 VLP (CAS 1317-70-0), nanopowder, ≥99.0%, from Kronos International, Inc. (Leverkusen, Germany); TiO_2 Mirkat 211 (CAS 1317-70-0), nanopowder, ≥99.0%, from MirkaTiO_2 (Italy); methyltriethoxysilane (MTES; CAS 2031-67-6), reagent grade, ≥98%, from Sigma-Aldrich® (Merck Life Science S.r.l., Milan, Italy); hydrochloric acid (HCl; CAS 7647-01-0), Puriss. p.a., ACS reagent, 37%, from Sigma-Aldrich® (Merck Life Science S.r.l., Milan, Italy); acetic acid (CH_3COOH; CAS 64-19-7), for HPLC, ≥99.8%, from Sigma-Aldrich® (Merck Life Science S.r.l., Milan, Italy); chitosan, medium molecular weight (CAS 9012-76-4), derived from Icelandic sources, from Sigma-Aldrich® (Merck Life Science S.r.l., Milan, Italy); *Origanum compactum* essential oil (EO), purchased from Pranarôm International S.A. (Ghislenghien, Belgium).

2.2. Matrix synthesis and coating formulation

2.2.1. Synthesis of MCM-41

The synthesis of silica mesoporous MCM-41 was performed using a procedure previously reported by the authors [47–49]. Briefly, MCM-41 was synthesized using TEOS as a silica source in an alkaline medium with CTAB as a template in NaOH basic solution. The molar ratio of the reagents is 1 SiO_2: 0.12 CTAB: 0.53 NaOH: 590H_2O. The mixture was stirred, aged, and then calcined at 510 °C with a rate of 0.5 °C/min in flowing air (50 mL min^{-1}) for 6 h to remove the template and achieve the mesoporous structure.

2.2.2. Impregnation with oregano essential oil and TiO_2

The incipient wetness impregnation (IWI) method was employed to load MCM-41 with 20 wt% of TiO_2. The IWI was performed using three commercially available TiO_2 samples: Evonik P25, Kronos VLP, and Mirkat 211. The main features of these three materials are reported in Table 1 [50–53]. The TiO_2-enriched MCM-41 samples were respectively labeled as MT (MCM-41 with Evonik P25), MM (MCM-41 with Mirkat 211), and MK (MCM-41 with Kronos VLK).

MCM-41 was also impregnated with the *Origanum compactum* essential oil (EO), leading to a concentration of 1.6 mL g^{-1}, once dried at T < 30 °C. The *O. compactum* essential oil was chosen for its antimicrobial and biocide properties [54–56]. The material was thus labeled as MO.

A third material was prepared by a double-steps impregnation of MCM-41 first with *O. compactum* essential oil and then with Evonik P25 TiO_2, following the same procedure previously described. The sample prepared was thus labeled as MOT (MCM-41 with oregano EO and Evonik P25 TiO_2).

2.2.3. Formulation of protective coating

A hybrid organic-inorganic hydrogel was selected as the best-suited

Table 1
Textural properties of commercial titania samples.

Sample	Specific surface area (m^2 g^{-1})	Pore size range (nm)	Pore volume (mL g^{-1})	Crystallite size (nm)	Band gap (eV)	Crystal phase
Evonik P25	52	4-80	0,13	40	3.15	Rutile and anatase
MIRKAT 211	217	4-10	0,27	11	3.25	Anatase
KRONOS VLP	269	4-10	0,30	15	3.21	Anatase

matrix for supporting the MOT material. For the organic component, attention was focused on the use of the biopolymer chitosan, whereas for the inorganic part, a mixture of 70:30 of MTES and TEOS was employed as silicium source in the sol-gel process (Fig. 1).

For this preparation, 0.7 mL of MTES and 0.3 mL of TEOS were mixed in 4 mL of CH_3COOH 0.1 M solution with two drops of 0.2 M HCl, acting as the gelation catalyst. Then it was subjected to ultrasonic treatment for 40 min to initiate hydrolysis and condensation reactions. 40 mg of MOT were then added, and the suspension was ultrasonicated for 1 h. In parallel, 30 mg of chitosan powder were dissolved in 3.5 mL of CH_3COOH 0.1 M solution, where 1 mL of HCl 0.4 M was added to act as a gelation catalyst. The chitosan solution was stirred at 800-900 rpm for 1 h until complete dissolution [57].

Finally, the MTES-TEOS mixture containing MOT was added to the chitosan solution. The resulting formulation was stirred at 300 rpm for 30 min to ensure interaction between the silica network and the chitosan. This process resulted in the formation of the hybrid hydrogel protective coating.

The final formulation was then labeled as C-MOT. As a reference for C-MOT, hydrogels were prepared using only MO, MT, and without any mesoporous SiO_2. These three formulations were therefore labeled C-MO, C-MT, and C, respectively. For clarity, the different coating formulation components are summarized in Table 2.

Table 2
Composition of the different coating formulations, where the full dot (●) represents the presence of the component, whereas the empty one (○) represents its absence.

Coating name	Hydrogel chitosan/ MTES-TEOS	MCM-41	*Origanum compactum* EO	TiO_2
C	●	○	○	○
C-MO	●	●	●	○
C-MT	●	●	○	●
C-MOT	●	●	●	●

2.3. Characterization of the SiO_2-TiO_2 samples

2.3.1. N_2 physisorption technique

The nitrogen physisorption technique was employed to study specific surface areas and pore size distributions of the materials by evaluating N_2 adsorption/desorption isotherms at −196 °C using a Tristar II Plus Micromeritics instrument. The samples underwent a pre-treatment at 200 °C before the analysis. The surface area was calculated using the B.E.T. method, whereas pore size distribution was determined by the B.J.H. method, applied to the N_2 desorption branch of the isotherm. For all the surface area data the error reported is lower than 2%.

2.3.2. Electron microscopy techniques

Scanning Electron Microscopy (SEM), coupled with Energy Dispersive X-ray Spectroscopy (EDS), and High-Resolution Transmission Electron Microscopy (HR-TEM) analyses were employed to study the morphological modification of the silica matrices, to study the nanostructured pores' dimensions, and to confirm the addition of the TiO_2. The analyses were conducted using a Zeiss Gemini SEM equipped with an Oxford Instruments SDD EDS detector and a JEOL 2100 HRTEM with a Gatan OneView detector. SEM images were gained at an accelerating voltage of 5 kV with the secondary electron detector, while EDS maps were captured at an accelerating voltage of 10 kV. SEM sample preparation involved spreading a thin layer of powdered sample onto adhesive conductive carbon tape. HRTEM imaging was carried out at an accelerating voltage of 200 kV. For HRTEM samples, the material was sonicated in ethanol for 5 min, then drop-cast onto a holey carbon copper grid (Agar Scientific) and left to air drying overnight. Data was collected using the Electron Microscopy Research Technology Platform at the University of Warwick.

2.4. Photocatalytic activity tests

The photocatalytic efficiency was evaluated by measuring the degradation under UV light of methylene blue (MB), chosen as model standard compound sensitive to photocatalytic degradation [58,59]. UV-visible spectroscopy was finally employed to monitor the degradation process, further details are reported in the Supplementary Information relative section [60,61].

The test was conducted as follows: [58,59] 125 mL of standard aqueous solution of MB $1x10^{-5}$ M was placed under magnetic stirring at 350 rpm. In the absence of illumination, 20 mg of the sample was poured into the MB solution and left stirring for 15 min until a homogeneous solution was obtained. The solution was then irradiated with a 125 W mercury UV lamp with an irradiance at the sample level of 40 W m^{-2} (spectral range 315-400 nm, HG100; Jelosil Srl) and 5 mL of the solution was withdrawn at regular intervals (0, 5, 10, 20, 40, 60, 90, 120 min). All samples were diluted with 5 mL of Milli-Q water and finally analyzed to monitor the degradation of MB over time with a Cary5000 UV-Vis spectrophotometer (200-800 nm wavelength range) by Agilent Technologies [62,63]. All data sets were processed with the software OriginPro 2021 by OriginLab, Northampton, MA, USA.

2.5. Application of the protective coating formulations

The coatings were applied in sterile conditions on previously sterilized white Carrara marble and green marble mock-ups and on laboratory-prepared concrete mock-ups. The concrete mock-ups were composed of sand, lime, and cement in a ratio of 4:2:1; the curing took place at room temperature and humidity; their treatment took place 30 days after the preparation to ensure complete curing. For each mock-up, the top surface was treated with 0.021 mL/cm^2 of product. The application was carried out using a roller to ensure consistent and even application of the coatings. These mock-ups were prepared using silicone molds, obtaining 5 x 5 × 2.5 cm samples. The marble mock-ups, also of surface 5 x 5, were sterilized by a 60-min cycle at 120 °C in an autoclave (HICLAVE HV, 110 L, HMC Europe) to then carry out microbiological tests.

2.6. Evaluation of the protective coating formulations properties

Once the coatings were applied to the mock-ups, hydrophobicity tests and colorimetric analyses were carried out to evaluate the properties of the formulations. Furthermore, antimicrobial properties were

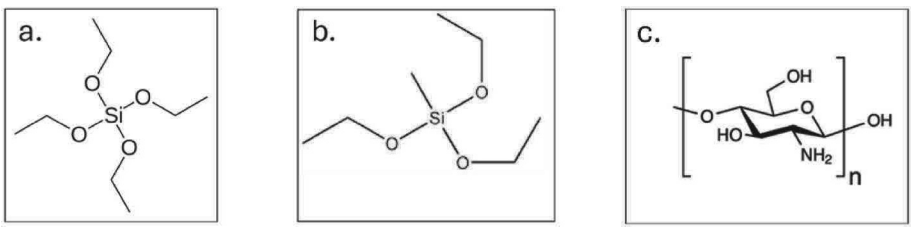

Fig. 1. Chemical structures of TEOS (a), MTES (b), and chitosan monomer (c).

studied by inoculating two fungal strains on the stone surfaces and observing their growth behavior.

2.6.1. Hydrophobicity and water vapor permeability tests

The hydrophobic properties of the surfaces were investigated by measuring the contact angle, following the UNI EN 15802 standard [64]. Briefly, 10 μL of deionized H_2O was deposited on the surfaces and after 10 s registered with a Celestron Deluxe Digital Handheld Microscope. The related contact angle was subsequently calculated, using ImageJ software.

The water vapor permeability test was carried out following the procedure described in the UNI EN 15803 standard [65]. In summary, the mock-ups were placed in a container, with 50 mL of a 93% KNO_3 solution, and sealed with microcrystalline wax, a refined paraffin. The test was performed both on treated and untreated mock-ups to compare the water vapor permeability. The weight of each sample was registered daily, as well as the Relative Humidity (RH%) and the temperature.

2.6.2. Colorimetric analysis

Color measurements were conducted with a Konica Minolta CM-26dG spectrophotometer both before and after the application of the protective coating. Results were elaborated by the software Spectra Magic NX. The total color variation, expressed as ΔE, was calculated by the following equation (1):

$$\Delta E = \sqrt{\Delta L^{*2} + \Delta a^{*2} + \Delta b^{*2}} \quad (1)$$

here ΔL^*, Δa^* and Δb^* represent the differences in the respective color coordinates between measurements taken before and after coating application.

To evaluate both the effectiveness of the protective coating and its long-term durability, additional measurements were taken after 9 months of natural ageing. The protection efficacy was assessed measuring the color differences between the aged and the untreated samples, whereas to determine the durability, color differences were calculated between the aged and the coated samples.

All colorimetric evaluations were based on Specular Component Included (SCI) data.

2.6.3. Antimicrobial properties

For this test *Penicillium chrysogenum* and *Aspergillus niger*, both fungi Ascomycota Eurotiales, were chosen as model pathogen microorganisms. In particular, the two fungi come from a real-case scenario in Ca' Cappello, also known as Palazzo Cappello Layard, a historical palace part of the Ca' Foscari University of Venice. The fungi were sampled non-invasively by sterile swabs and allowed to grow in pure culture in Petri dishes (Ø = 100 mm) with a Sabouraud Dextrose Agar (SDA), microbiological grade, from Sigma-Aldrich® (Merck Life Science S.r.l., Milan, Italy) cultivation medium in an incubator (VELP, Refrigerated Thermostats FOC 225E) at 18 °C for 7 days, reaching an optimal inoculation growth level with active sporulating conidiophores.

The test was based on a system, consolidated by the authors, used for monitoring fungal growth [66,67]. Specifically, to evaluate the antimicrobial activity of the various formulation treatments, each coated mock-up was placed in a sterile cylindrical container filled with SDA growth medium up to the surface level of the mock-up. Once the medium was solidified, it was inoculated with 1 mL of fungal spore solution (approx. 500 ± 25 spores mL^{-1}), and the container was covered with a cotton and aluminum foil lid and secured with an elastic band. Fig. 2 shows the main components of the setup. All the parts were sterilized in an autoclave (HICLAVE HV, 110 L, HMC Europe) for 60 min at a temperature of 120 °C before the test was started.

The containers were monitored at room temperature for up to 60 days, with pictures taken at regular intervals (2, 7, 14, 35, and 60 days) to evaluate fungal growth. Then, the images were analyzed in post-production using the image management software of the Nikon SMZ800N stereomicroscope, adjusting contrast and scale where necessary to allow consistent qualitative comparison of fungal growth. At the end, a sampling by Fungi-Tape™ was carried out on the center of the mock-ups to microscopically evaluate the fungal growth.

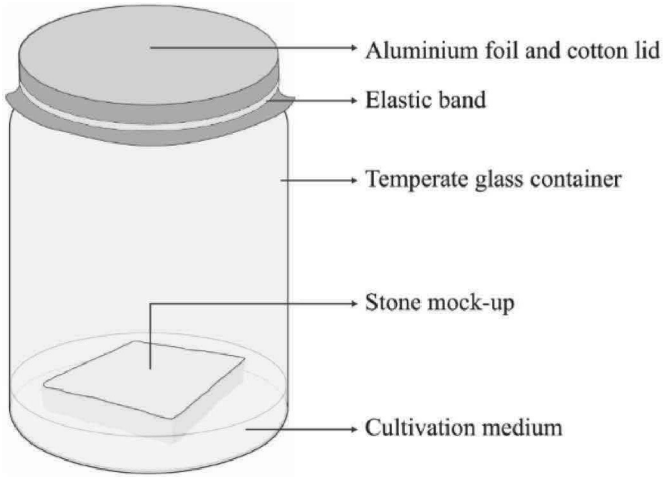

Fig. 2. Schematic representation of the system set-up for the microbiological test.

For this test white Carrara marble and green marble mock-ups were employed, repeating the test in triplicate ($n = 3$). C-MOT coating was tested, keeping as reference the mock-ups treated with C-MO, C-MT, C, and some uncoated ones.

3. Results

3.1. Characterization of the SiO_2/TiO_2 material MT

The isotherms and pore size distributions of the SiO_2/TiO_2 sample MT are compared with the ones of MCM-41 in Fig. 3a and b, respectively. The surface area, average pore diameter, and pore volume of the samples are reported in Table 3. The same measurements for samples MM and MK are reported in the supplementary information (Fig. S1 and Table S1). The nitrogen physisorption analysis of the MCM-41 sample confirms its successful synthesis, exhibiting an average pore diameter of 2.7 nm, a high surface area of 1249 $m^2\ g^{-1}$, and a well-defined mesoporous structure, as evidenced by its characteristic Type IV isotherm and hysteresis loop. For the titania-impregnated sample MT, the isotherms maintain a Type IV shape but with reduced adsorbed gas volume. The widening and partial change in the shape of the loop can be associated with a change in the size of the mesopores, making them less available, likely due to the partial blockage of the pores by the titania nanoparticles [68]. To account for the coexistence of the titania NPs and MCM-41 silica in the material both contributing to the overall physisorption profile, a comparison with the TiO_2 isotherm profile was taken as a reference (Fig. 2S).

Overall, the addition of titania allowed the maintenance of proper surface area and porosity values without significantly compromising the silica texture. This is essential for photocatalytic applications as it ensures adequate adsorption surface area. Comparable behavior is also evident in the other TiO_2-enriched samples reported in Table S1. To further confirm these results, electron microscopy analyses were conducted.

Fig. 4a displays a HRTEM micrograph of the MCM-41 sample, highlighting an overall well-defined morphology, and uniform shapes, indicative of a highly ordered morphology of the SiO_2 particles. Fig. 4b provides instead a higher magnification view, focusing on the arrangement of the mesoporous channels within the MCM-41 sample, showing a periodic arrangement of pores. The regular, hexagonal pattern of the pores confirms the successful formation of the mesoporous silica

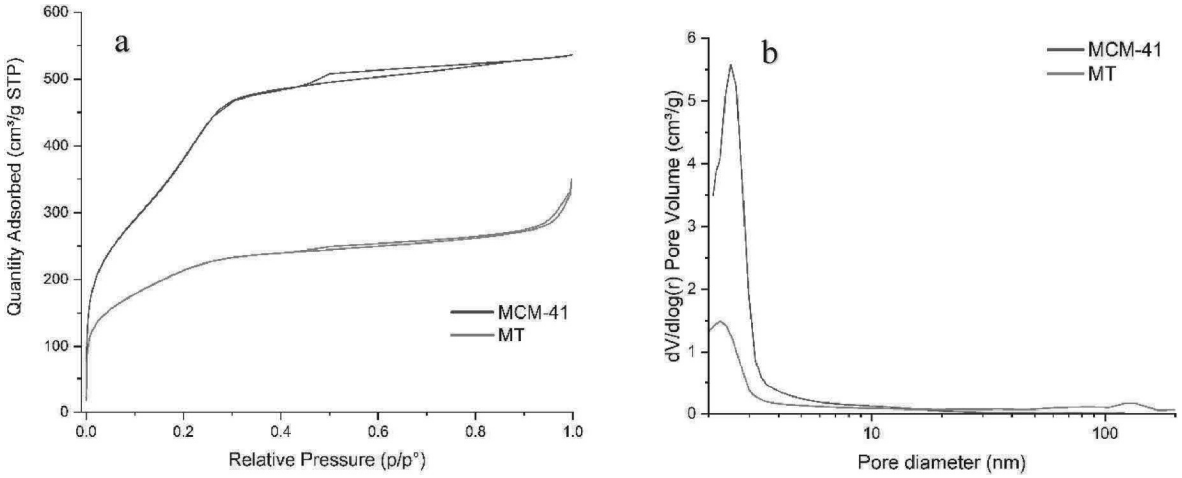

Fig. 3. N_2 adsorption-desorption isotherm (a) and pore diameter distribution (b) of MCM-41 and MT samples.

Table 3
Specific area, average pore size, and pore volume of MCM-41 and MT.

	Surface area ($m^2\ g^{-1}$)	Pore diameter (nm)	Pore volume ($cm^3\ g^{-1}$)
MCM-41	1249	2.49	0.85
MT	763	2.25	0.45

framework. This hexagonal packing is a defining characteristic of MCM-41, indicating the material's high degree of structural regularity.

The micrograph of MT sample (Fig. 4c) reveals an excellent structural integrity preservation of the MCM-41 structure post-impregnation with the TiO_2 nanoparticles. Of particular interest are the distinct and parallel lattice fringes, which suggest the presence of crystalline TiO_2 on the silica surface, partially covering it. These fringes are indicative of well-dispersed TiO_2 nanoparticles, likely in the anatase or rutile phase. The HRTEM analysis confirms that the MCM-41 structure remains unaffected by the impregnation with the TiO_2 and its ordered nature is preserved. A similar behavior can be observed also in the other TiO_2-enriched samples in Fig. S3.

The SEM micrograph of MCM-41, presented in Fig. 5, shows particles with spherical shapes, consistent with the expected morphology of MCM-41. The surface texture appears mostly smooth, with minor irregularities. The size (ranging from 100 to 500 nm) and shape of the

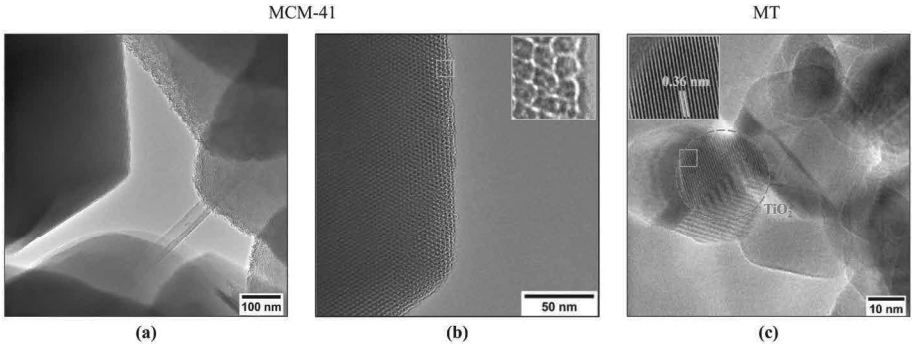

Fig. 4. HRTEM micrographs of MCM-41 (**a** and **b**) and MT (**c**) samples.

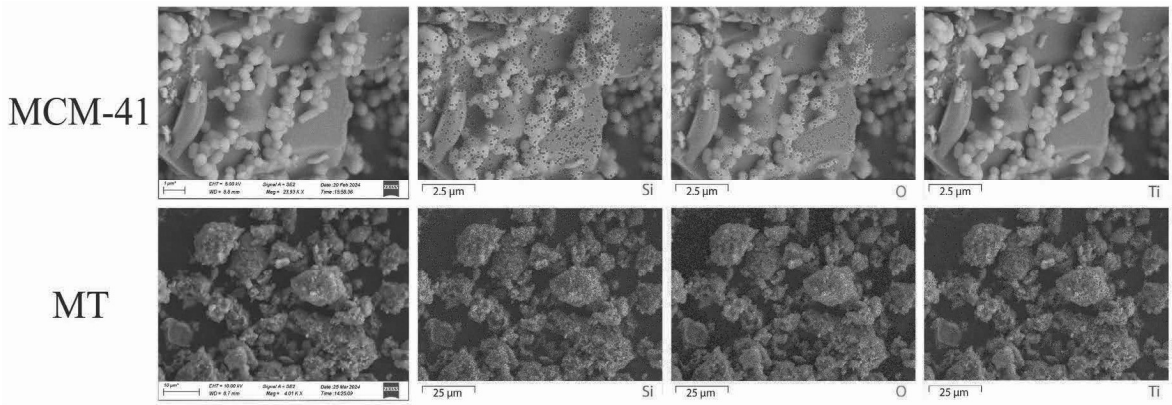

Fig. 5. SEM micrographs of MCM-41 and MT, overlapped to the EDS maps identifying Silicon (blue marked), Oxygen (green marked), and Titanium (purple marked).

material are critical factors influencing the properties of the final protective coating, such as transparency, hydrophobicity, homogeneity, and viscosity. Specifically, the spherical shape could significantly affect the roughness of the final coating, which subsequently reduces wettability and increases water repellency [69,70].

The same characteristics can be found in the samples impregnated with TiO_2, for which SEM micrographs can be found in Fig. S4, where the uniform distribution of titanium can be observed in the EDS maps corresponding to the SEM micrographs. The consistent Ti signal across the sample suggests that TiO_2 is homogeneously distributed on the external surface of the silica material; if TiO_2 NPs were confined to the internal pores, its signal would likely appear less uniform and more localized to specific regions. The EDS maps also reveal an overlapping presence of Si and O across all the samples. Silicon, associated with the MCM-41 framework, and oxygen, present in both silica and titania structures, demonstrate the thorough integration of titania within the silica matrix.

3.2. Photocatalytic activity test

To evaluate the photoactivity of the TiO_2/SiO_2 composite materials and ensure that it was maintained after interaction with *Origanum compactum* essential oil (EO), the samples were tested for their ability to degrade Methylene Blue (MB) under UV light. From a preliminary evaluation of the photoactivity of the tested silica/titania materials (see Fig. S5), the most efficient one was found to be Evonik P25, so the study was focused only on it. This result was correlated to the presence of a double crystalline phase of Evonik P25, in comparison to the other photocatalysts. Fig. 6 illustrates the MB degradation profiles for pure MCM-41, MT, and MOT samples, with degradation efficiency plotted as MB's relative concentration (C/C_0) over time.

As highlighted by the steepest decline in MB concentration, the MT sample showed photocatalytic activity achieving nearly complete methylene blue degradation within 60 min. MOT maintained photocatalytic activity but required 5 h to completely degrade the MB; the initial methylene blue concentration decrease in MOT suggests significant adsorption on the material's surface and pores, though the presence of the EO slightly hindered MB diffusion to titania active sites, slowing degradation.

This process is governed by two simultaneous mechanisms: adsorption and degradation. Therefore, not only the photocatalytic properties but also the surface area of the materials used play a crucial role. For instance, MCM-41, despite lacking photocatalytic properties, still showed a slight decrease in the concentration of methylene blue through an adsorption mechanism by its mesoporous structure. This adsorption removed methylene blue molecules from the solution, leading to an apparent decrease in concentration. These two mechanisms act in combination, leading to a general discoloration of the solution. Nevertheless, observing the residual solid SiO_2, it is possible to partially discriminate the results: the TiO_2 NPs provide active sites for photocatalysis upon exposure to light, resulting in the degradation of methylene blue molecules not only in the solution but also once absorbed. The solid SiO_2 residue is initially blue, but then it whitens as the degradation of MB goes on (see Fig. S6 and the *Photocatalytic activity test* section in the supplementary information).

Concluding, it is possible to state that despite this slower rate, the essential oil did not block the photocatalytic activity of the TiO_2, as the titania nanoparticles, located on the MOT material's surface, continued to promote methylene blue degradation under UV light. Thus, the preserved photocatalytic efficiency of MOT made the material suitable for application in the protective coating formulation.

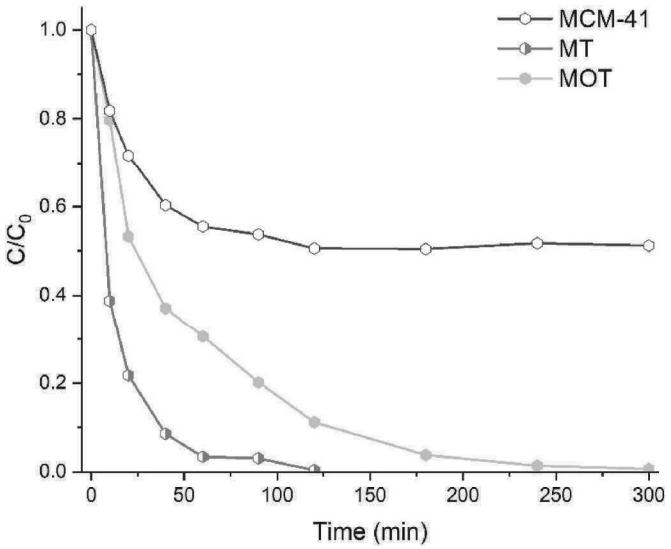

Fig. 6. Graph of the degradation of Methylene Blue under UV light using MCM-41, MT and MOT.

3.3. Evaluation of the protective coating formulation properties

The MCM-41 nanocapsules with oregano EO and Evonik P25 TiO_2 were embedded in the chitosan and MTES/TESO matrix protective coating formulation, named C-MOT. After applying it to the surface of the mock-ups, various tests were conducted to assess the coating's properties.

3.3.1. Hydrophobicity and water vapor permeability measures

Table 4 reports the contact angle measurements before and after the treatment of the three different substrates and the measurements after nine months of natural ageing. Further details, including pictures of the droplets, are reported in Table S2 in the SI.

Before the treatments, the mock-ups behave differently depending on the substrate characteristics. Concrete contains a hydrated cement paste mainly composed of calcium silicates and aluminates (C-S-H and C-A-H), which generates a network of pores and capillaries. This porous structure makes concrete inherently hydrophilic. Marble, on the other hand, has a compact crystalline structure based on calcium carbonate which, despite exhibiting a certain moderate porosity, is more effective at inhibiting water penetration. As a result, the untreated concrete mock-up shows a contact angle of 0° while the marbles are 70° and 58°.

After treatment, the contact angle of the concrete mock-up rises sharply from 0° to 90°. A similar trend is observed in the marble mock-ups: the contact angle increases from 70° to 87° for white Carrara marble and from 58° to 86° for green marble. These results indicate a marked improvement in hydrophobicity following the coating treatment.

This enhanced hydrophobicity can be mainly attributed to the hydrogel formulation. The nonpolar side chains (methyl groups) of MTES increase surface hydrophobicity, while spherical mesoporous SiO_2 particles may further contribute by introducing microroughness, which reduces the effective contact area between water and the substrate. A qualitatively similar mechanism occurs on superhydrophobic surfaces (as described by the Cassie–Baxter model), where air trapped within the

Table 4
Contact angle values of the sample surfaces before and after the application of the C-MOT coating and before and after the natural ageing treatment, in comparison with the not treated mock-ups.

Material	Before treatment	After treatment	After Ageing
Treated Concrete	0.0°	90° ± 1	84° ± 1
Not treated Concrete		*n.a.*	0.0°
Treated White Marble	70° ± 1	88° ± 1	81° ± 1
Not treated White Marble		*n.a.*	53° ± 1
Treated Green Marble	58° ± 1	86° ± 1	66° ± 1
Not treated Green Marble		*n.a.*	35° ± 1

surface roughness prevents water from fully making contact with the surface [71].

Further hydrophobicity measurements were performed on aged mock-ups to assess the effectiveness of the coating over time and to compare the loss of contact angle between treated and untreated surfaces. The results clearly show that the coating significantly enhances and preserves hydrophobicity across all substrates. On concrete, untreated samples remained completely wettable (0°), while treated ones reached 90° after application and still maintained a high value of 84° after ageing, indicating very good durability. For white marble, the coating increased the contact angle from 70° before treatment to 88°, whereas untreated aged samples only reached 53°. Even after ageing, treated white marble retained a much higher contact angle (81°), demonstrating the protective effect of the coating. Green marble exhibited the largest decrease after ageing, dropping from 86° to 66°; however, this value remains substantially higher than the untreated aged sample (35°). Overall, these comparisons highlight that the coating provides a consistent improvement in water repellency, with concrete showing the most stable long-term performance, white marble retaining moderate durability, and green marble being the most affected by ageing yet still clearly outperforming untreated surfaces.

These promising increase in surface hydrophobicity after the treatment need to be considered along with the water vapor permeability ones, since these two parameters are strictly connected.

Fig. 7 represents a histogram with the water vapor permeability (δ_p) data of the three materials before and after the application of the C-MOT coating treatment. It is possible to notice a slight decrease in permeability after the application, but in all cases lower than 20%; keeping in mind that the UNI EN 15803 standard does not establish a fixed percentage threshold for the acceptable variation in water vapor permeability after the application of a protective treatment. However, in the field of conservation and according to best restoration practices, a reduction in water vapor permeability of less than 30-40% compared to the untreated material is generally considered acceptable [9,72].

Another interesting aspect that can be noticed is the high difference in water vapor permeability between the concrete and the marble samples. This difference can be attributed to the diverse composition of the materials and can be correlated to other characteristics, such as the porosity, which for concrete is usually around 10-20%, whereas for marble is between 0.3% and 1.5% [73–75].

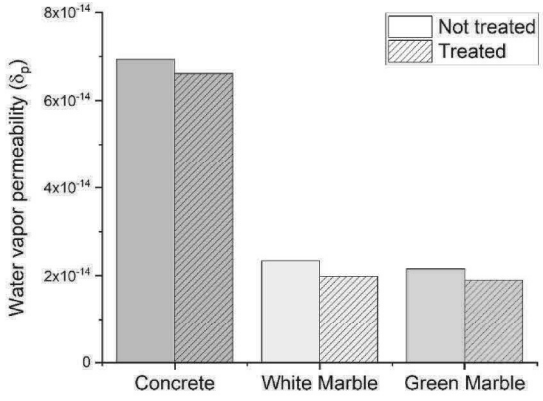

	Decrease in δ_p (%)
Concrete	4.6 %
White Carrara Marble	15.4 %
Green Marble	11.6 %

Fig. 7. Histogram of the water vapor permeability values (δ_p) with relative decrease % of each material underneath.

3.3.2. Colorimetric analyses

To examine potential chromatic alterations following the coating application and to evaluate its aesthetic stability over time, colorimetric analyses were performed. Measurements were taken at three distinct points on the mock-ups' surface during three different time periods, which corresponded to three distinct ΔE metrics: *ΔE application* (calculated comparing the surface appearance before and after the application of the coating), *ΔE ageing* (calculated comparing the surface appearance before and after the ageing of the samples), and *ΔE protection* (calculated comparing the surface appearance before the application of the coating and after the ageing).

Table 5 presents the average ΔE values of *ΔE application* and *ΔE ageing*, while detailed colorimetric data in the CIE Lab* color space are reported in Table S3 and Table S4.

Examining the average *ΔE application*, it is evident that the color variation is below the detection threshold of the naked human eye ($\Delta E > 3$). This indicates that the application of the protective coating does not significantly change the appearance of the substrates.

For *ΔE ageing*, the average color variation after the ageing process also remains below 3, demonstrating that the coating maintains its aesthetic stability over at least nine months of outdoor exposure.

The *ΔE protection* was used to evaluate the effectiveness and durability of the protective coating after ageing. It was calculated both for treated samples and for untreated samples subjected to the ageing process.

As illustrated in Fig. 8, untreated mock-ups exhibited a significant color change due to the natural ageing, whereas the treated samples showed lower variation. This highlights the protective efficacy of the coating in mitigating chromatic alterations over time.

Considering the overall experimental evidence and the characterization performed on the C-MOT coating formulation and its constituent materials, it is possible to state that a protective coating with promising features was developed for application on various stone substrates. The TiO_2/SiO_2 materials exhibited good homogeneity and a strong ability to degrade model stain compounds, even when combined with oregano essential oil. Furthermore, once incorporated into the hydrogel formulation, it demonstrated excellent performance, enhancing hydrophobicity without significantly altering the water vapor permeability or aesthetics of the surface, even after ageing, showing efficiency and stability over time. To finally validate the formulation features, an in-depth study of the coating components' antimicrobial activity was necessary.

3.4. Evaluation of the antimicrobial activity

The monitoring of fungal growth of both molds *Penicillium chrysogenum* and *Aspergillus niger* on pristine white Carrara and green marble mock-ups revealed rapid growth in the cultivation medium during the first few days, followed by a stationary growth phase once the marble surfaces became partially covered.

Table 6 presents pictures of one mock-up of each type, inoculated with *P. chrysogenum* or *A. niger*, over the 60-day period.

Regarding *P. chrysogenum* colonization on white marble, widespread coverage is observed by day 14, with complete colonization confirmed

Table 5
Average ΔE values of the stone mock-ups before and after treatment (pristine vs coated) and before and after ageing (treated vs aged) with relative Standard Deviation (SD).

Material	Average ΔE coating application	SD	Average ΔE coating ageing	SD
Concrete	3	0.5	3	0.9
White Marble	3	0.5	3	0.5
Green Marble	3	0.8	3	0.5

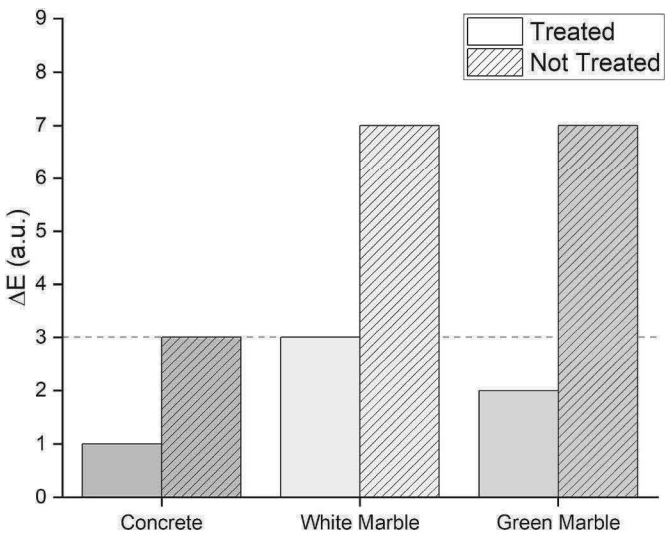

Fig. 8. Histogram of the color variation values (ΔE protection) comparing the treated and not treated mock-ups.

by day 60. This well-established colonization is further evidenced by the release of pigments onto the stone surface, which takes on a yellowish color, a characteristic effect of *P. chrysogenum* [76,77]. Although no visible color change is appreciable in the green marble mock-up, a similar growth pattern emerges, with fungal development already noticeable on the surface by day 14.

For *A. niger* on white marble, complete surface coverage is observed within the first 7 days, with dark spots (*i.e.* conidiophores) becoming evident and intensifying over time. By day 14, the white surface begins to take on a yellowish hue, which gradually darkens to a brownish coloration by day 60. *A. niger* is known to produce brown and yellowish pigments, such as melanin, which may be then absorbed by the marble substrate [78,79]. In contrast, no color change is appreciable in the green marble mock-up, although a speckled appearance emerges from day 14 and becomes more intense by day 60, suggesting a similar growth pattern.

For comparison, Table 7 presents the pictures of the mock-ups treated with the final C-MOT formulation, which consists of a chitosan-MTES/TEOS hydrogel and MCM-41 SiO_2 impregnated with *Origanum compactum* essential oil and enriched with Evonik P25 TiO_2 NPs. As before, the cultivation medium surrounding both marble mock-ups was inoculated with *P. chrysogenum* or *A. niger*. These images reveal a stark contrast to the untreated samples. While *P. chrysogenum* growth is still noticeable in some areas, *A. niger* development is significantly inhibited.

Analyzing the pictures of the mock-ups inoculated with *P. chrysogenum*, it is evident that the C-MOT formulation effectively inhibits fungal colonization from day 14. This period could be associated with favorable atmospheric precipitation conditions, which may facilitate the washout and subsequent removal of colonizing spores from the stone surface. However, in later images, particularly those of the white Carrara marble mock-ups, a slight yellowing of the surface is observed, suggesting that the formulation might not completely prevent fungal growth or that pigments produced by the fungi in the cultivation medium may have penetrated the substrate from the sides.

In contrast, the mock-ups inoculated with *A. niger* exhibit a near-total inhibition of fungal growth when treated with the C-MOT formulation. By the end of the 60-day monitoring period, the samples remain almost free of fungal coverage, even though the surfaces of the substrates treated with this coating exhibit a light pale-yellow hue.

To fully understand the role of the formulation's different components, the positive results obtained with C-MOT were compared with those obtained with C, C-MT, and C-MO formulations. This approach allows us to differentiate the influence of the chitosan-MTES/TEOS hydrogel from that of *Origanum compactum* essential oil and Evonik P25 TiO_2 nanoparticles. Since the clearest results were previously obtained with the white Carrara marble mock-ups, this material was selected as the reference for comparison.

From Table 8, it can be observed that the mock-ups treated with the C formulation exhibit a low level of colonization after 14 days. However, some dark spots begin to appear, and by day 60, the surface darkens with a yellowish tone. When silica and TiO_2 are added (C-MT formulation), a reduction in colonization is observed at day 14. However, this is not sufficient to prevent the surface yellowing, as seen in the pictures taken on day 60, particularly in the case of *A. niger*.

Examining the C-MO formulation, it was observed that even after 60 days, the mock-up surfaces appear free of fungal colonization. However, a comparison with the C-MOT formulation pictures reveals that the latter maintains a cleaner surface with lighter tones.

The antimicrobial effectiveness of the four different coating formulations, each tested to assess the contribution of individual components, was evaluated quantitatively in an indirect way. For safety reasons, images taken during the growth of the two inoculated Fungi were analyzed in post-production using the image management software of the Nikon SMZ800N stereomicroscope This approach allowed validation of the qualitative visual observations through precise colorimetric data. Based on the growth dynamics observed during monitoring, mold development ranges were then assigned, establishing macroscopic parameters summarized in Table 9.

The application of this strategy facilitated a more direct comparison of the effectiveness of the four different coatings, corroborating the visual evidence that had already emerged and had been previously discussed. The development trend of the mold *A. niger* on both Carrara White Marble and Green Marble is shown in Fig. 9, while that of *P. chrysogenum* is shown in Fig. 10. In both cases, the reported values represent the mean of three independent measurements per sample, with a standard deviation consistently below 5% ($n = 3$, SD $< \pm 5\%$).

Considering these findings, it is likely that the primary active component in the C-MOT formulation responsible for inhibiting fungal growth is *Origanum compactum* essential oil. The active antimicrobial molecules in this extract, once encapsulated in mesoporous MCM-41 silica, are released over an extended period, exerting a prolonged inhibitory effect on fungal proliferation, both regarding the development of the vegetative mycelium and the initiation of a sporulation phase. This sustained activity is attributed to the physical and morphological characteristics of the mesoporous SiO_2 carrier, which enables controlled release of the active compounds. The addition of TiO_2 nanoparticles (NPs) also enhances the overall antimicrobial activity, as titania possesses biocidal properties, as demonstrated in the C-MT coating. However, in the C-MT formulation, the antimicrobial activity of titania may not be sufficiently strong or fully exploited. This limitation may be due to the absence of direct UV radiation, which is often necessary to activate titania's full photocatalytic potential. Testing under UV radiation was not feasible in this study, as it would have independently influenced fungal proliferation.

Nonetheless, in the C-MOT coating, the combined inhibitory effects of encapsulated *Origanum compactum* essential oil and TiO_2 nanoparticles result in a synergistic antimicrobial action, enhancing overall effectiveness. Therefore, the combination of both active components in C-MOT presents a promising strategy for developing durable antimicrobial coatings, particularly for cultural heritage conservation and other applications requiring persistent biodeteriogens prevention.

4. Conclusions

Within this work a nanostructured, photocatalytic, multifunctional coating was developed based on a chitosan-MTES/TEOS hydrogel, embedding mesoporous MCM-41 silica loaded with titanium dioxide and *Origanum compactum* essential oil. This innovative formulation

Table 6
Photographs taken at 2, 7, 14, 28, 35, and 60 days after the inoculation on pristine mock-ups.

	PRISTINE WHITE MARBLE		PRISTINE GREEN MARBLE	
Penicillium chrysogenum	 Day 2	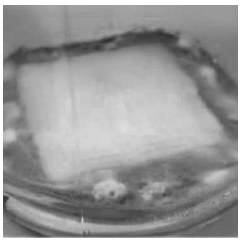 Day 28	 Day 2	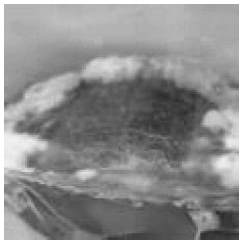 Day 28
	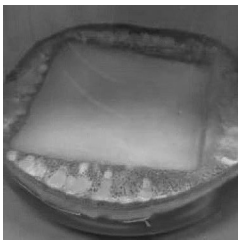 Day 7	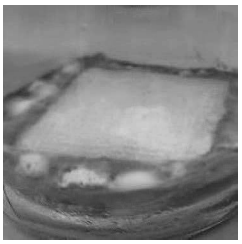 Day 35	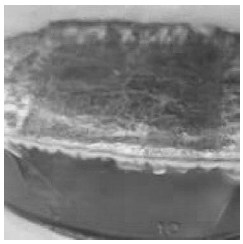 Day 7	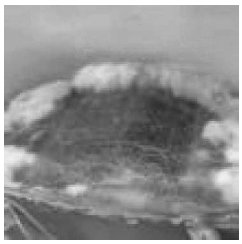 Day 35
	 Day 14	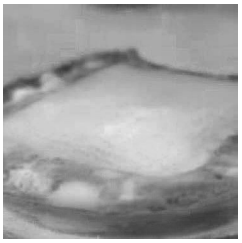 Day 60	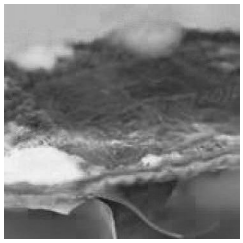 Day 14	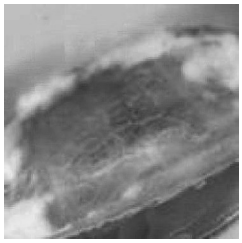 Day 60
Aspergillus niger	 Day 2	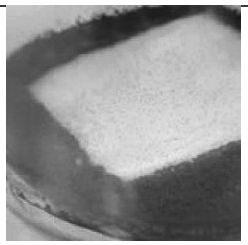 Day 28	 Day 2	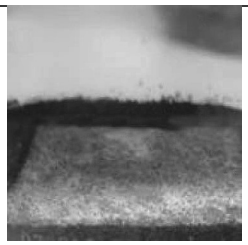 Day 28
	 Day 7	 Day 35	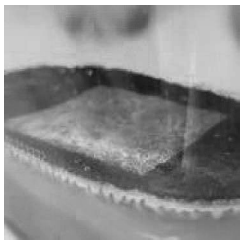 Day 7	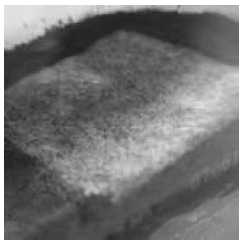 Day 35
	 Day 14	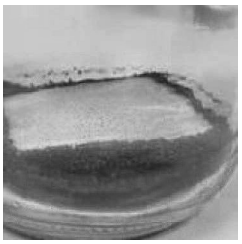 Day 60	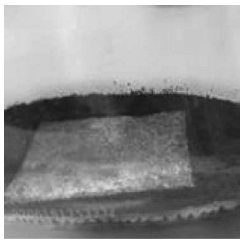 Day 14	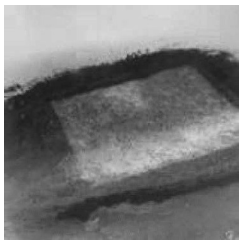 Day 60

Table 7
Photographs taken at 2, 7, 14, 28, 35, and 60 days after the inoculation on mock-ups treated with C-MOT.

	WHITE MARBLE TREATED WITH C-MOT		GREEN MARBLE TREATED WITH C-MOT	
Penicillium chrysogenum	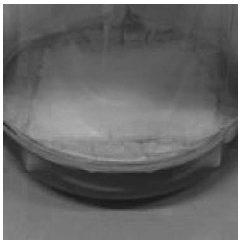 Day 2	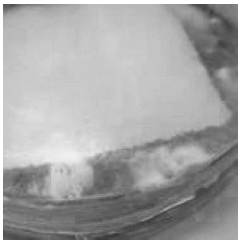 Day 28	 Day 2	 Day 28
	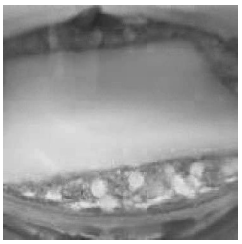 Day 7	 Day 35	 Day 7	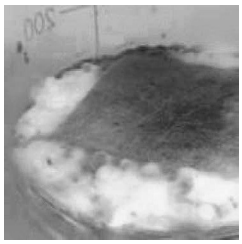 Day 35
	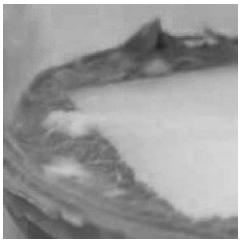 Day 14	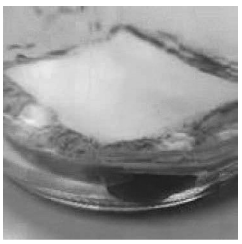 Day 60	 Day 14	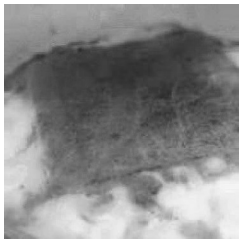 Day 60
Aspergillus niger	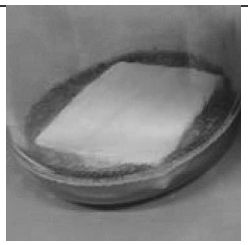 Day 2	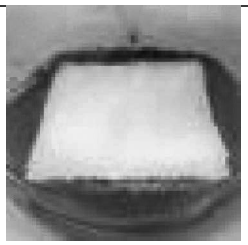 Day 28	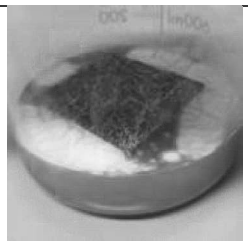 Day 2	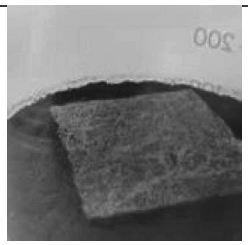 Day 28
	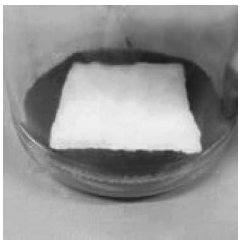 Day 7	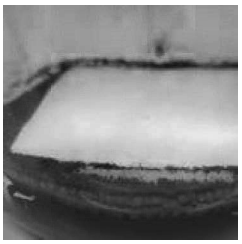 Day 35	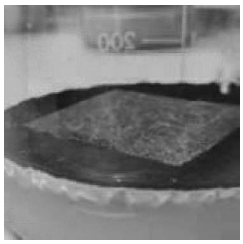 Day 7	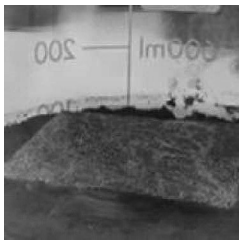 Day 35
	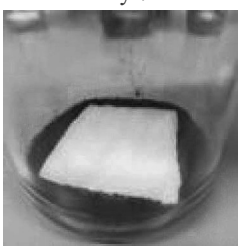 Day 14	 Day 60	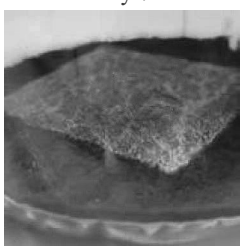 Day 14	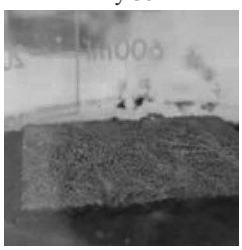 Day 60

Table 8
Photographs taken after 14 and 60 days from inoculation of *Penicillium chrysogenum* and *Aspergillus niger* fungi with white Carrara marble mock-ups previously treated with the different coating formulations.

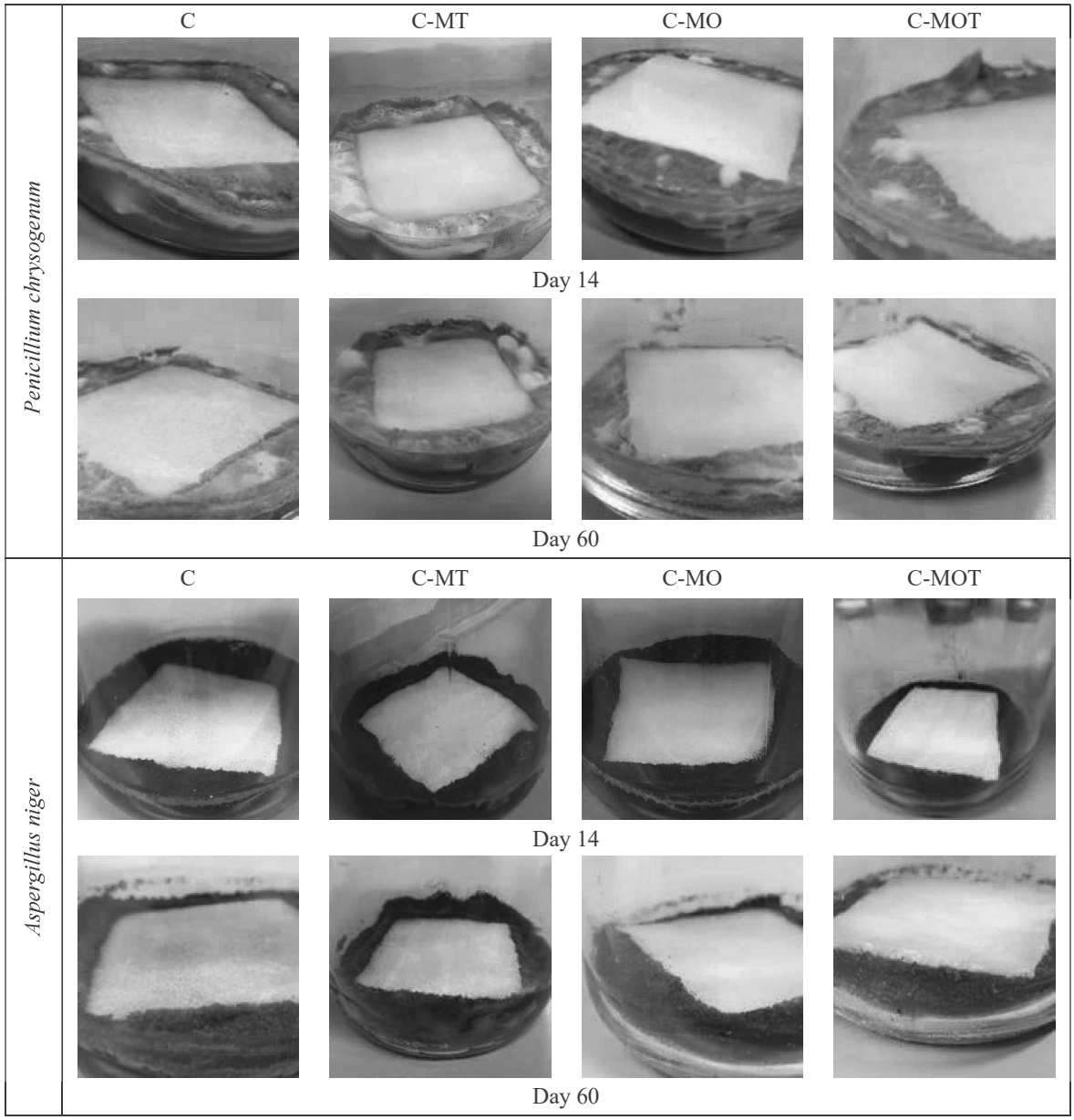

Table 9
Macroscopic parameters assigned to identify the ranges of stone mock-up's surface biocolonization, expressed as % coverage, occurring in a centripetal direction (from edge to center of the mock-up).

Biocolonized surface (%)	Description
0-1%	*absence of biocolonization or presence of some conidiophores*
<1-15%	*approximately 2-3* mm *marginal biocolonization*
<16-30%	*approximately 10-15* mm *marginal biocolonization*
<30-50%	*biocolonization of approximately 20-30* cm *from the mock-up's edge*
<50-70%	*uneven biocolonization: presence of conidiophores in spots up to mock-up's center*
<70-80%	*almost total biocolonization*
<80-100%	*total biocolonization of the substrate (both sterile and vegetative mycelium)*

provides a multifunctional and synergistic antimicrobial effect, combining the slow release of the essential oil from the mesoporous silica, thanks to its textural and surface features properties, with the photocatalytic activity of titanium dioxide, which enhance the biocidal effect and is also well known for its ability to degrade pollutants.

The hybrid hydrogel matrix, combining silica alkoxides and chitosan, proved to be an effective carrier for both the nanoparticles and the essential oil, ensuring uniform filming formation, appropriate viscosity properties, and good adhesion to the stone surface. The coating not only protects the surface from pollution and microbial degradation phenomena but also provides hydrophobicity to the surface while maintaining water vapor permeability and color stability.

Overall, these results demonstrate the potential of this multifunctional photocatalytic coating as a sustainable and effective strategy for stone material preservation, offering enhanced protection against microbial degradation, environmental pollutants, and moisture without

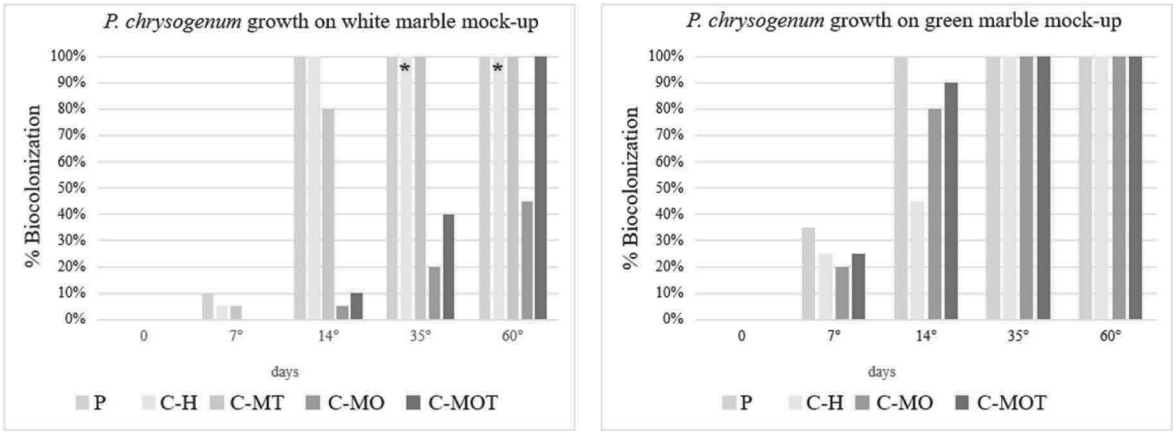

Fig. 9. Comparison (n = 3, SD < ±5%) between the percentages of biocolonization of *Aspergillus niger* on pristine (P) and C, C-MT, C-MO, and C-MOT coated mock-ups in white (on the left) and green (on the right) marble. Release of marked pigmentation on stone mock-up's surface by Fungi is reported as (*).[NB Refer to Table 9 for the determination of the identified biocolonization ranges].

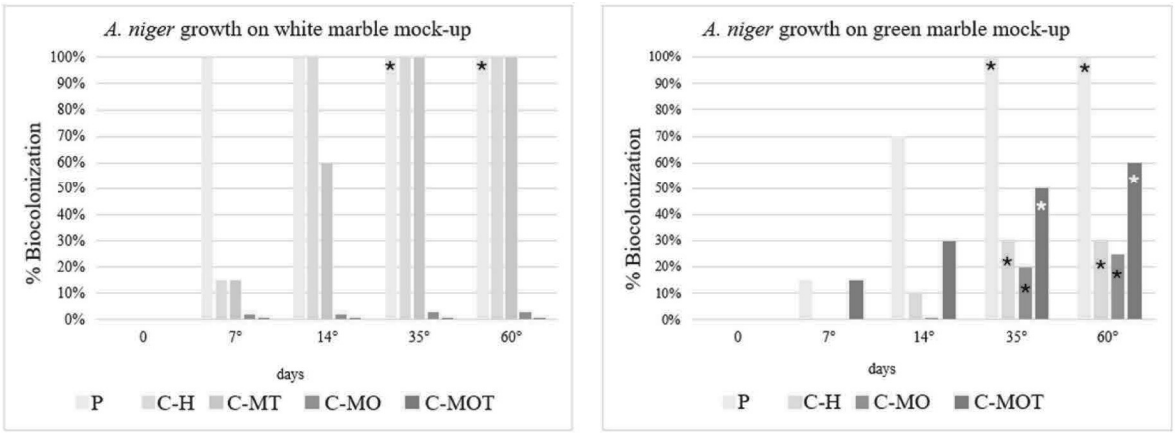

Fig. 10. Comparison (n = 3, SD < ±5%) between the percentages of biocolonization of *Penicillium chrysogenum* on pristine (P) and C, C-MT, C-MO, and C-MOT coated mock-ups in white (on the left) and green (on the right) marble. Release of marked pigmentation on stone mock-up's surface by Fungi is reported as (*). [NB Refer to Table 9 for the determination of the identified biocolonization ranges].

compromising the aesthetic and structural integrity of the substrate.

Declaration of generative AI and AI-assisted technologies in the writing process

During the preparation of this work the authors used DeepL Write in order to improve language and readability. After using this tool, the authors reviewed and edited the content as needed and take full responsibility for the content of the publication.

CRediT authorship contribution statement

Andrea Campostrini: Conceptualization, Data curation, Formal analysis, Investigation, Methodology, Writing – original draft. **Teresa Botrè:** Formal analysis. **Elena Ghedini:** Data curation, Methodology, Validation, Writing – review & editing. **Sabrina Manente:** Methodology, Validation. **Alex W. Robertson:** Formal analysis. **Pilar Bosh-Roig:** Methodology, Validation. **Federica Menegazzo:** Conceptualization, Data curation, Funding acquisition, Methodology, Supervision, Validation, Writing – review & editing. **Michela Signoretto:** Funding acquisition, Supervision.

Declaration of competing interest

The authors declare that they have no known competing financial interests or personal relationships that could have appeared to influence the work reported in this paper.

Acknowledgments

The authors would like to thank Ms. Valentina A. Rizzolio for her practical contributions to part of this work and acknowledge the financial support of the "PON Research and Innovation 2014–2020", the "Fund for the Promotion and Development of PNR Policies 2021–2027", and the restoration company *Uni.S.Ve. Srl* of Venice (Italy) for financing Andrea Campostrini's PhD scholarship.

Appendix A. Supplementary data

Supplementary data to this article can be found online at https://doi.org/10.1016/j.mtsust.2026.101367.

Data availability

Data will be made available on request.

References

[1] B.J. Smith, M. Gomez-Heras, S. McCabe, Understanding the decay of stone-built cultural heritage, Prog. Phys. Geogr. Earth Environ. 32 (2008) 439–461, https://doi.org/10.1177/0309133308098119.

[2] K. Elert, C. Rodriguez-Navarro, Degradation and conservation of clay-containing stone: a review, Constr. Build. Mater. 330 (2022) 127226, https://doi.org/10.1016/j.conbuildmat.2022.127226.

[3] M. Tokmak, M. Dal, Classification of physical, chemical and biological deteriorations observed in Ankara stone monuments, Int. J. Pure Appl. Sci. 6 (2020) 8–16, https://doi.org/10.29132/ijpas.718466.

[4] E. Sesana, A.S. Gagnon, C. Ciantelli, J. Cassar, J.J. Hughes, Climate change impacts on cultural heritage: a literature review, WIREs Clim. Change 12 (2021) e710, https://doi.org/10.1002/wcc.710.

[5] P.N. Manoudis, I. Zuburtikudis, G. Konstantopoulos, H.A. Khalifeh, C. Kottaridi, I. Karapanagiotis, Superhydrophobicity, photocatalytic self-cleaning and biocidal activity combined in a siloxane-ZnO composite for the protection of limestone, Biomimetics 9 (2024) 573, https://doi.org/10.3390/biomimetics9090573.

[6] S. Centenaro, G. Franceschin, E. Cattaruzza, A. Traviglia, Consolidation and coating treatments for glass in the cultural heritage field: a review, J. Cult. Herit. 64 (2023) 132–143, https://doi.org/10.1016/j.culher.2023.09.006.

[7] Y. Ocak, A. Sofuoglu, F. Tihminlioglu, H. Böke, Protection of marble surfaces by using biodegradable polymers as coating agent, Prog. Org. Coat. 66 (2009) 213–220, https://doi.org/10.1016/j.porgcoat.2009.07.007.

[8] A. Makhmetova, E.-S. Negim, D. Ainakulova, G. Yeligbayeva, J. Khatib, An overview of Epoxy Resins as coating to protect metals from corrosion, Kompleksnoe Ispol'zovanie Mineral'nogo Syr'â/Complex Use of Mineral Resources 328 (2024) 20–32, https://doi.org/10.31643/2024/6445.03.

[9] R. Lamuraglia, A. Campostrini, E. Ghedini, A. De Lorenzi Pezzolo, A. Di Michele, G. Franceschin, F. Menegazzo, M. Signoretto, A. Traviglia, A new green coating for the protection of frescoes: from the synthesis to the performances evaluation, Coatings 13 (2023) 277, https://doi.org/10.3390/coatings13020277.

[10] A. Artesani, F. Di Turo, M. Zucchelli, A. Traviglia, Recent advances in protective coatings for cultural Heritage–An overview, Coatings 10 (2020) 217, https://doi.org/10.3390/coatings10030217.

[11] T. Warscheid, J. Braams, Biodeterioration of stone: a review, Int. Biodeterior. Biodegrad. 46 (2000) 343–368, https://doi.org/10.1016/S0964-8305(00)00109-8.

[12] P.S. Griffin, N. Indictor, R.J. Koestler, The biodeterioration of stone: a review of deterioration mechanisms, conservation case histories, and treatment, Int. Biodeterior. 28 (1991) 187–207, https://doi.org/10.1016/0265-3036(91)90042-P.

[13] N.S. Geweely, New frontiers review of some recent conservation techniques of organic and inorganic archaeological artefacts against microbial deterioration, Front. Microbiol. 14 (2023) e1146582, https://doi.org/10.3389/fmicb.2023.1146582.

[14] I.A. Jones, L.T. Joshi, Biocide use in the antimicrobial era: a review, Molecules 26 (2021) 2276, https://doi.org/10.3390/molecules26082276.

[15] S.A. Ruffolo, M.F. La Russa, Nanostructured coatings for stone protection: an overview, Front. Mater. 6 (2019) e00147, https://doi.org/10.3389/fmats.2019.00147.

[16] M. Roveri, F. Gherardi, S. Goidanich, D. Gulotta, V. Castelvetro, R. Fischer, L. Winandy, J. Weber, L. Toniolo, Self-cleaning and antifouling nanocomposites for stone protection: properties and performances of stone-nanomaterial systems, IOP Conf. Ser. Mater. Sci. Eng. 364 (2018) 012070, https://doi.org/10.1088/1757-899X/364/1/012070.

[17] I. Franco-Castillo, L. Hierro, J.M. de la Fuente, A. Seral-Ascaso, S.G. Mitchell, Perspectives for antimicrobial nanomaterials in cultural heritage conservation, Chem 7 (2021) 629–669, https://doi.org/10.1016/j.chempr.2021.01.006.

[18] F. Gherardi, P.N. Maravelaki, *Advances in the application of nanomaterials for natural stone conservation*, RILEM Tech, Lett. 7 (2022) 20–29, https://doi.org/10.21809/rilemtechlett.2022.159.

[19] Y. Wei, Q. Wu, H. Meng, Y. Zhang, C. Cao, Recent advances in photocatalytic self-cleaning performances of TiO2-based building materials, RSC Adv. 13 (2023) 20584–20597, https://doi.org/10.1039/D2RA07839B.

[20] M. Dell'Edera, C. Lo Porto, I. De Pasquale, F. Petronella, M.L. Curri, A. Agostiano, R. Comparelli, Photocatalytic TiO2-based coatings for environmental applications, Catal. Today 380 (2021) 62–83, https://doi.org/10.1016/J.CATTOD.2021.04.023.

[21] H. Shu, M. Yang, Q. Liu, M. Luo, Study of TiO2-Modified sol coating material in the protection of stone-built cultural heritage, Coatings 10 (2020) 179, https://doi.org/10.3390/coatings10020179.

[22] B. Yang, Z. Ma, Q. Wang, J. Yang, Synthesis and photoelectrocatalytic applications of TiO2/ZnO/Diatomite composites, Catalysts 12 (2022) 268, https://doi.org/10.3390/catal12030268.

[23] A.-I. Gopalan, J.-C. Lee, G. Saianand, K.-P. Lee, P. Sonar, R. Dharmarajan, Y. Hou, K.-Y. Ann, V. Kannan, W.-J. Kim, Recent progress in the abatement of hazardous pollutants using photocatalytic TiO2-Based building materials, Nanomaterials 10 (2020) 1854, https://doi.org/10.3390/nano10091854.

[24] O.M. Ishchenko, V. Rogé, G. Lamblin, D. Lenoble, TiO2- and ZnO-Based materials for photocatalysis: material properties, device architecture and emerging concepts, in: Semiconductor Photocatalysis – Materials, Mechanisms and Applications, InTech, 2016, https://doi.org/10.5772/62774.

[25] F. Pinzari, Synthesis, photocatalytic and bio activity of ZnO-TiO2 nanocomposites: a review study, Reactions 5 (2024) 680–739, https://doi.org/10.3390/reactions5040035.

[26] S. Veltri, A.M. Palermo, G. De Filpo, F. Xu, Subsurface treatment of TiO2 nanoparticles for limestone: prolonged surface photocatalytic biocidal activities, Build. Environ. 149 (2019) 655–661, https://doi.org/10.1016/J.BUILDENV.2018.10.038.

[27] A. Campostrini, S. Manente, E. Ghedini, A. Di Michele, F. Menegazzo, Enhancing Venetian traditional marmorino with TiO2 and ZnO for antimicrobial protection – a case study, Next Mater. 7 (2025) 100384, https://doi.org/10.1016/j.nxmate.2024.100384.

[28] J. Cai, R. Yan, J. Shi, J. Chen, M. Long, W. Wu, K. Kuca, Antifungal and mycotoxin detoxification ability of essential oils: a review, Phytother Res. 36 (2022) 62–72, https://doi.org/10.1002/ptr.7281.

[29] M.A. Kakakhel, F. Wu, J.-D. Gu, H. Feng, K. Shah, W. Wang, Controlling biodeterioration of cultural heritage objects with biocides: a review, Int. Biodeterior. Biodegrad. 143 (2019) 104721, https://doi.org/10.1016/j.ibiod.2019.104721.

[30] M.R. Fidanza, G. Caneva, Natural biocides for the conservation of stone cultural heritage: a review, J. Cult. Herit. 38 (2019) 271–286, https://doi.org/10.1016/j.culher.2019.01.005.

[31] A. Mutlu-Ingok, D. Devecioglu, D.N. Dikmetas, F. Karbancioglu-Guler, E. Capanoglu, Antibacterial, antifungal, antimycotoxigenic, and antioxidant activities of essential oils: an updated review, Molecules 25 (2020) 4711, https://doi.org/10.3390/molecules25204711.

[32] J. Trovão, A. Portugal, Current knowledge on the fungal degradation abilities profiled through biodeteriorative plate essays, Appl. Sci. 11 (2021) 4196, https://doi.org/10.3390/app11094196.

[33] G. Ranalli, E. Zanardini, C. Sorlini, Biodeterioration – including cultural heritage, in: Reference Module in Life Sciences, Elsevier, 2018, https://doi.org/10.1016/B978-0-12-809633-8.13016-X.

[34] F.A. Arzani, J.H.Z. dos Santos, Biocides and techniques for their encapsulation: a review, Soft Matter 18 (2022) 5340–5358, https://doi.org/10.1039/D1SM01114F.

[35] S.K. Sundar, J.K. Parikh, Advances and trends in encapsulation of essential oils, Int. J. Pharm. 635 (2023) 122668, https://doi.org/10.1016/j.ijpharm.2023.122668.

[36] L. Ruggiero, F. Bartoli, M.R. Fidanza, F. Zurlo, E. Marconi, T. Gasperi, S. Tuti, L. Crociani, E. Di Bartolomeo, G. Caneva, M.A. Ricci, A. Sodo, Encapsulation of environmentally-friendly biocides in silica nanosystems for multifunctional coatings, Appl. Surf. Sci. 514 (2020) 145908, https://doi.org/10.1016/j.apsusc.2020.145908.

[37] M. Peng, L. Wang, L. Guo, J. Guo, L. Zheng, F. Yang, Z. Ma, X. Zhao, A durable Nano-SiO2-TiO2/Dodecyltrimethoxysilane superhydrophobic coating for stone protection, Coatings 12 (2022) 1397, https://doi.org/10.3390/coatings12101397.

[38] Y. Liu, J. Liu, Design of multifunctional SiO2–TiO2 composite coating materials for outdoor sandstone conservation, Ceram. Int. 42 (2016) 13470–13475, https://doi.org/10.1016/j.ceramint.2016.05.137.

[39] C. Kapridaki, P. Maravelaki-Kalaitzaki, TiO2–SiO2–PDMS nano-composite hydrophobic coating with self-cleaning properties for marble protection, Prog Org Coat 76 (2013) 400–410, https://doi.org/10.1016/j.porgcoat.2012.10.006.

[40] L. Toniolo, F. Gherardi, The protection of marble surfaces: the challenge to develop suitable nanostructured treatments, in: Advanced Materials for the Conservation of Stone, Springer International Publishing, Cham, 2018, pp. 57–78, https://doi.org/10.1007/978-3-319-72260-3_3.

[41] K. Wang, N. Bu, Q. Zhen, J. Liu, S. Bashir, Modified nano-SiO2/TiO2 hybrid fluorinated B-72 as antimicrobial and hydrophobic coatings for the conservation of ancient bricks, Constr. Build. Mater. 365 (2023) 130090, https://doi.org/10.1016/j.conbuildmat.2022.130090.

[42] A. Bakhshian Nik, H. Zare, S. Razavi, H. Mohammadi, P. Torab Ahmadi, N. Yazdani, M. Bayandori, N. Rabiee, J. Izadi Mobarakeh, Smart drug delivery: capping strategies for mesoporous silica nanoparticles, Microporous Mesoporous Mater. 299 (2020) 110115, https://doi.org/10.1016/j.micromeso.2020.110115.

[43] Z. Alothman, A review: fundamental aspects of silicate mesoporous materials, Materials 5 (2012) 2874–2902, https://doi.org/10.3390/ma5122874.

[44] R. Narayan, U. Nayak, A. Raichur, S. Garg, Mesoporous silica nanoparticles: a comprehensive review on synthesis and recent advances, Pharmaceutics 10 (2018) 118, https://doi.org/10.3390/pharmaceutics10030118.

[45] M. Zuena, L. Ruggiero, G. Caneva, F. Bartoli, G. Della Ventura, M.A. Ricci, A. Sodo, Assessment of stone protective coatings with a novel eco-friendly encapsulated biocide, Coatings 11 (2021) 1109, https://doi.org/10.3390/coatings11091109.

[46] A. Ramirez, J.-M. Clacens, C. Lorentz, Y. Pouilloux, Comparison between SBA-15 and MCM-41 structure on the stability and the selectivity of basic catalysts in oligomerization of glycerol, Curr. Org. Chem. 16 (2012) 2774–2781, https://doi.org/10.2174/138527212804546903.

[47] A. Breda, M. Signoretto, E. Ghedini, F. Pinna, G. Cruciani, Acylation of veratrole over promoted SZ/MCM-41 catalysts: influence of metal promotion, Appl. Catal. A: Gen. 308 (2006) 216–222, https://doi.org/10.1016/j.apcata.2006.04.039.

[48] W. Zeng, X.-F. Qian, J. Yin, Z.-K. Zhu, The drug delivery system of MCM-41 materials via co-condensation synthesis, Mater. Chem. Phys. 97 (2006) 437–441, https://doi.org/10.1016/j.matchemphys.2005.08.040.

[49] A. Campostrini, E. Ghedini, T. Botrè, S. Manente, A. Giordana, G. Cerrato, G. Cruciani, A.W. Robertson, M. Signoretto, F. Menegazzo, Engineered silica NPs to hold and release the antimicrobial product biotin T®, Next Mater. 7 (2025) 100373 https://doi.org/10.1016/j.nxmate.2024.100373.

[50] T. Vrålstad, W.R. Glomm, G. Øye, J. Sjöblom, M. Stöcker, Cobalt functionalization of mesoporous silica by incipient wetness impregnation and co-precipitation, J. Dispers. Sci. Technol. 26 (2005) 87–94, https://doi.org/10.1081/DIS-200040230.

[51] T.M. Albayati, G.M. Alwan, O.S. Mahdy, High performance methyl orange capture on magnetic nanoporous MCM-41 prepared by incipient wetness impregnation method, Korean J. Chem. Eng. 34 (2017) 259–265, https://doi.org/10.1007/s11814-016-0231-2.

[52] A. Das, M. Patra, R.R. Wary, P. Gupta, R.G. Nair, Photocatalytic performance analysis of Degussa P25 under various laboratory conditions, in: IOP Conf. Ser.: Mater. Sci. Eng., vol 377, IOP Publ, 2018 012101, https://doi.org/10.1088/1757-899X/377/1/012101.
[53] E. Ghedini, F. Menegazzo, M. Manzoli, A. Di Michele, D. Puglia, M. Signoretto, Multifunctional and environmentally friendly TiO2-SiO2 mesoporous materials for sustainable green buildings, Molecules 24 (2019) e243427, https://doi.org/10.3390/molecules24234226.
[54] A.S. Doost, C.V. Stevens, M. Claeys, P. Van Der Meeren, Fundamental study on the salt tolerance of oregano essential oil-in-water nanoemulsions containing tween 80, Langmuir 35 (2019) 10572–10581, https://doi.org/10.1021/acs.langmuir.9b01620.
[55] H. Mith, R. Duré, V. Delcenserie, A. Zhiri, G. Daube, A. Clinquart, Antimicrobial activities of commercial essential oils and their components against food-borne pathogens and food spoilage bacteria, Food Sci. Nutr. 2 (2014) 403–416, https://doi.org/10.1002/fsn3.116.
[56] H. Mith, A. Clinquart, A. Zhiri, G. Daube, V. Delcenserie, The impact of oregano (Origanum heracleoticum) essential oil and carvacrol on virulence gene transcription by Escherichia coli O157:H7, FEMS Microbiol. Lett. 362 (2015), https://doi.org/10.1093/femsle/fnu021 fnu021.
[57] M. Signoretto, F. Menegazzo, E. Ghedini, Medical or Cosmetic Compounds, and Composition Thus Obtained, 2019. WO2019215592A1.
[58] C.H. Kwon, H. Shin, J.H. Kim, W.S. Choi, K.H. Yoon, Degradation of methylene blue via photocatalysis of titanium dioxide, Mater. Chem. Phys. 86 (2004) 78–82, https://doi.org/10.1016/j.matchemphys.2004.02.024.
[59] D. Zanardo, E. Ghedini, F. Menegazzo, A. Giordana, G. Cerrato, A. Di Michele, G. Cruciani, M. Signoretto, Traditional Venetian marmorino: effect of zinc-based oxides on self-bleaching properties, J. Cult. Herit. 50 (2021) 171–178, https://doi.org/10.1016/J.CULHER.2021.04.006.
[60] F.S. Rocha, A.J. Gomes, C.N. Lunardi, S. Kaliaguine, G.S. Patience, Experimental methods in chemical engineering: ultraviolet visible Spectroscopy-UV-Vis, Can. J. Chem. Eng. 96 (2018) e23344, https://doi.org/10.1002/cjce.23344.
[61] C.S. Uyguner, M. Bekbolet, Evaluation of humic acid photocatalytic degradation by UV-vis and fluorescence spectroscopy, Catal. Today 107 (2005) 78–82, https://doi.org/10.1016/j.cattod.2005.03.011.
[62] G. Ferraro, A. Di Vera, E. Ghedini, M. Marchiori, G. Forghieri, P. Canton, M. Signoretto, Carbon-dots-conjugated semiconductors for enhanced solar-driven photocatalysis, Appl. Catal. O: Open 192 (2024) 206942, https://doi.org/10.1016/j.apcato.2024.206942.
[63] L. Scappin, A. Campostrini, D. Zanardo, E. Ghedini, M. Signoretto, G. Berto, F. Menegazzo, Marmorino and photocatalysts: a meeting between tradition and innovation, Int. J. Architectural Conserv. Restor. I (2022) 35–49.
[64] UNI Ente Italiano di Normazione, Home – UNI Ente Italiano di Normazione, (n.d.), accessed June 5 2024, https://store.uni.com/.
[65] UNI Ente Italiano di Normazione, Home – UNI Ente Italiano di Normazione, (n.d.), accessed June 4 2024, https://store.uni.com/.
[66] A. Campostrini, A. Sala-Luis, P. Bosch-Roig, E. Ghedini, M. Signoretto, F. Menegazzo, Mesoporous silica and vegetal extracts combined as sustainable stone heritage protection against biodeterioration, Appl. Microbiol. Biotechnol. 109 (2025) 99, https://doi.org/10.1007/s00253-025-13475-5.
[67] M. del P. Bosch-Roig, A. Campostrini, A. Sala-Luis, Desarrollo de un recubrimiento sostenible elaborado por nanopartículas de sílice y biocidas naturales para la protección a largo plazo de superficies pétreas del patrimonio cultural frente al biodeterioro, Arché (2025) 106–109.
[68] A. Bhaumik, S. Samanta, N.K. Mal, Iron oxide nanoparticles stabilized inside highly ordered mesoporous silica, Pramana 65 (2005) 855–862, https://doi.org/10.1007/BF02704085.
[69] R.R. Castillo, L. de la Torre, F. García-Ochoa, M. Ladero, M. Vallet-Regí, Production of MCM-41 nanoparticles with control of particle size and structural properties: optimizing operational conditions during Scale-Up, Int. J. Mol. Sci. 21 (2020) 7899, https://doi.org/10.3390/ijms21217899.
[70] C.G. Sonwane, C.W. Jones, P.J. Ludovice, A model for the structure of MCM-41 incorporating surface roughness, J. Phys. Chem. B 109 (2005) 23395–23404, https://doi.org/10.1021/jp051713c.
[71] M.J. Mosquera, L.A.M. Carrascosa, N. Badreldin, Producing superhydrophobic/oleophobic coatings on cultural heritage building materials, Pure Appl. Chem. 90 (2018) 551–561, https://doi.org/10.1515/pac-2017-0404.
[72] E. Pargoletti, V. Comite, P. Fermo, V. Sabatini, L. Annunziata, M.A. Ortenzi, H. Farina, G. Cappelletti, Calcitic-based stones protection by a low-fluorine modified methacrylic coating, Environ. Sci. Pollut. Res. 29 (2022) 29455–29466, https://doi.org/10.1007/s11356-021-15515-9.
[73] E. Sassoni, E. Franzoni, Influence of porosity on artificial deterioration of marble and limestone by heating, Appl. Phys. A 115 (2014) 809–816, https://doi.org/10.1007/s00339-013-7863-4.
[74] E.S.R. Lasheen, M.A. Rashwan, M.K. Azer, Effect of mineralogical variations on physico-mechanical and thermal properties of granitic rocks, Sci. Rep. 13 (2023) 10320, https://doi.org/10.1038/s41598-023-36459-9.
[75] C. Lian, Y. Zhuge, S. Beecham, The relationship between porosity and strength for porous concrete, Constr. Build. Mater. 25 (2011) 4294–4298, https://doi.org/10.1016/j.conbuildmat.2011.05.4298.
[76] A. Viggiano, O. Salo, H. Ali, W. Szymanski, P.P. Lankhorst, Y. Nygård, R.A. L. Bovenberg, A.J.M. Driessen, Pathway for the biosynthesis of the pigment chrysogine by Penicillium chrysogenum, Appl. Environ. Microbiol. 84 (2018), https://doi.org/10.1128/AEM.02246-17.
[77] F. Fierro, I. Vaca, N.I. Castillo, R.O. García-Rico, R. Chávez, Penicillium chrysogenum, a vintage model with a cutting-edge profile in biotechnology, Microorganisms 10 (2022) 573, https://doi.org/10.3390/microorganisms10030573.
[78] Y. Qin, Y. Xia, Melanin in fungi: advances in structure, biosynthesis, regulation, and metabolic engineering, Microb. Cell Fact. 23 (2024) 334, https://doi.org/10.1186/s12934-024-02614-8.
[79] S.M. Koch, C. Freidank-Pohl, O. Siontas, M. Cortesao, A. Mota, K. Runzheimer, S. Jung, K. Rebrosova, M. Siler, R. Moeller, V. Meyer, Aspergillus niger as a cell factory for the production of pyomelanin, a molecule with UV-C radiation shielding activity, Front. Microbiol. 14 (2023) e1233740, https://doi.org/10.3389/fmicb.2023.1233740.